

Three-dimensional magneto-photoluminescence of multiply charged excitons in InAs/GaAs quantum dots coupled to a continuum of states

B. Van Hattem,^{1,*} P. Corfdir,¹ P. Brereton,^{1,†} P. Pearce,¹ A. M. Graham,¹
M. J. Stanley,¹ M. Hugues,^{2,‡} M. Hopkinson,² and R. T. Phillips.¹

¹*Cavendish Laboratory, University of Cambridge,
J. J. Thomson Avenue, CB3 0HE Cambridge, United Kingdom*

²*Department of Electronic and Electrical Engineering,
University of Sheffield, Mappin Street, Sheffield S1 3JD, United Kingdom*
(Dated: February 27, 2013)

We present a three-dimensional magneto-photoluminescence study on neutral and charged excitons confined to InAs/GaAs quantum dots. Our investigation relies on a confocal setup that allows tuning arbitrarily the angle between the applied magnetic field and the sample growth axis. First, from experiments on neutral excitons and trions, we extract the in-plane and on-axis components of the Landé tensor for electrons and holes in the s -shell. Then, based on the doubly negatively charged exciton magneto-photoluminescence we show that the p -electron wave function spreads significantly into the GaAs barriers. We also demonstrate that the p -electron g -factor depends on the presence of a hole in the s -shell. The magnetic field dependence of triply negatively charged excitons photoluminescence exhibits several anticrossings, as a result of coupling between the quantum dot electronic states and the wetting layer. Finally, we discuss how the system evolves from a Kondo-Anderson exciton description to the artificial atom model when the orientation of the magnetic field goes from Faraday to Voigt geometry.

I. INTRODUCTION

In the last fifteen years, quantum dots (QDs) have attracted a lot of interest from the scientific community as they allow for the development of a new class of quantum optoelectronic devices including single photon emitters¹, photon entangled pairs emitters^{2,3} or all-optical logic gates.⁴ Furthermore, recognition that the behaviour of QDs departs from the “artificial atom” model opens new areas of investigation involving the coupling between the discrete electronic states of the QD with a continuum.^{5–7} One of the most versatile ways of investigating the fine structure and the spin properties of electronic excitations confined to QDs is to study their three-dimensional response to a magnetic field.^{8–13} Magneto-photoluminescence experiments on excitons and trions have also proved successful in aiding estimation of the shape,^{14,15} the alloy composition,¹⁶ and the symmetry of QDs.^{17,18} Less is known about the magneto-photoluminescence of more negatively charged excitonic complexes.^{6,19} Still, the spectroscopy of such highly charged excitons makes it possible to study the interaction between charge carriers located in different shells.^{19–21} In addition, when three or more electrons are confined in the QD, applying a magnetic field may hybridize the QD electronic states with the Landau levels of the two-dimensional wetting layer.⁶

In this work, we present a magneto-photoluminescence (PL) study of charged excitons confined in InAs/GaAs QDs. Our experimental set-up permits arbitrary tuning of the angle between the applied magnetic field and the sample growth axis. This allows the study of the evolution of the diamagnetic shift of the excitonic complex with respect to the orientation of the field, providing in-

formation on the electron-hole correlation length of the exciton wave function, and the extraction of the in-plane and on-axis components of the electron and hole Landé g -factors. In the peculiar case of the doubly negatively charged exciton X^{2-} , we deduce from its magneto-PL that the p -shell electron wave function spreads significantly inside the GaAs barriers and that this spreading strongly depends on the presence of a hole in the s -shell. The triply negatively charged exciton X^{3-} is found to show PL that strongly deviates from the magnetic field dependence seen for the neutral exciton, the trions and the X^{2-} . We attribute this observation to the hybridization between the QDs electronic states with the wetting layer and we describe the evolution of this coupling as the magnetic field is rotated.

The paper is organized as follows. In Section II, we present the structure of our QD sample and we describe our confocal magneto-PL apparatus. In Section III, we identify by PL the different charge states of the exciton. In Section IV, we discuss the magneto-PL of the neutral exciton, the trions and the X^{2-} . Based on the magnetic field-dependence of the emission lines, we deduce in particular in Sections IV.A and IV.B the shape of the exciton wave function and the Landé tensor, respectively. In Section V, we present the magnetic-field dependence of the X^{3-} and we describe how the coupling of the final state of the recombination with the wetting layer affects the exciton recombination energies. We finally present our conclusions in Section VI.

II. EXPERIMENTAL DETAILS

The investigated InAs/GaAs QD sample has been grown by molecular beam epitaxy. The QDs are obtained

by the Stranski-Krastanov growth mode transition and are embedded in a field effect structure. The QD layer is located 25 nm above a n -doped GaAs substrate and 205 nm below a Schottky contact layer. We deposited on top of the structure a 40 nm gold mask patterned with apertures with 400 nm diameter. In order to access the different charged states of the QD, a voltage ranging between -0.8 and 0.15 V was applied to the Schottky structure. For all PL experiments, the sample was excited with a cw Ti:Al₂O₃ laser operating at 780 nm. In the case of PL experiments at zero magnetic field, the emitted light was sent to a triple spectrometer operating in additive mode (spectral resolution better than 20 μ eV) and was detected by a Peltier-cooled CCD. Magneto-PL experiments were carried out at 4.5 K in a confocal set-up, in which the confocal head is rotatable with respect to the field, as showed in Figure 1.²² This allows setting the angle θ between the sample growth axis and the applied magnetic field to any arbitrary value between 0 (Faraday geometry) and 90° (Voigt geometry). Magnetic fields up to 10 T have been obtained with a ‘dry’ superconducting magnet. We estimate the spectral resolution of our magneto-PL experiments to be better than 150 μ eV.

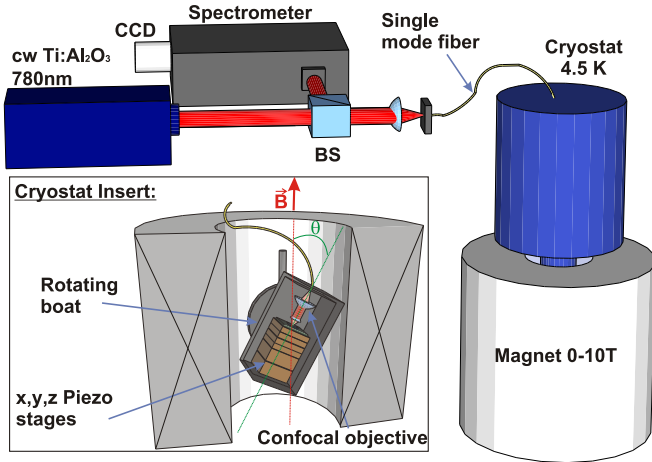


FIG. 1. (color online) Optical setup used for the magneto-photoluminescence measurements. The applied magnetic field is always along the vertical direction. Inset: the sample is mounted on a boat that can be rotated at any value of the angle θ within the magnet

III. IDENTIFICATION OF THE CHARGE STATES OF THE EXCITON

We show in Figure 2 the QD emission spectra at zero magnetic field for applied gate voltages between -0.8 to 0.15 V. We attribute the abrupt changes in the QD PL energy to the charging of the QD.²³ Using the method described in Ref.²¹, we identify the emission from the neutral exciton X^0 and from the singly, doubly and triply negatively charged excitons X^- , X^{2-} and X^{3-} , respec-

tively. Applying gate voltages larger than 0.1 V results in the filling of wetting layer states, making it impossible to observe the emission from QD exciton states more negatively charged than X^{3-} .^{23–26} When increasing the excitation density, additional lines become visible [Figure 2(b)]. We attribute them to the recombination of neutral and charged biexciton complexes²⁶ and to the emission from the positively charged trion X^+ .²⁷ Finally, we emphasize that the gate voltage of the charging steps are excitation dependent, which we ascribe to the modification of the effective electrostatic potential felt by the QD in presence of excess charges.

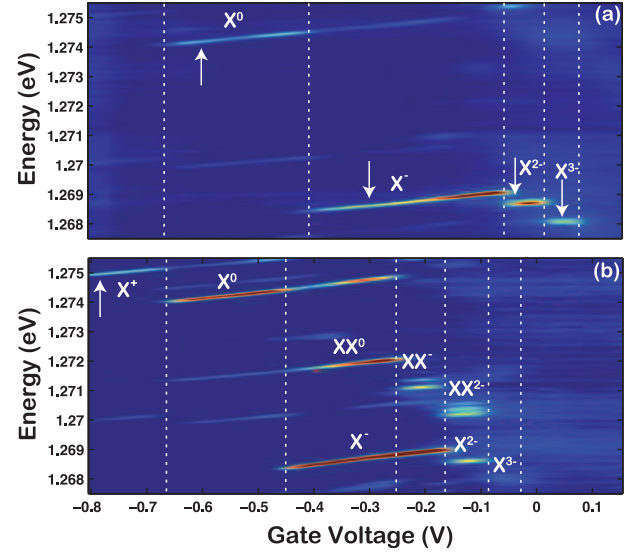


FIG. 2. (color online): QD emission spectra as a function of the gate voltage, for an excitation density of $5 \times 10^9 \mu\text{W}/\text{cm}^2$ (a) and $60 \times 10^9 \mu\text{W}/\text{cm}^2$ (b). Vertical dotted lines indicate the different charging steps. Arrows show at which voltage the magneto-PL scans in Figures 5, 6 and 7 have been taken.

IV. THREE-DIMENSIONAL MAGNETO-PHOTOLUMINESCENCE OF THE X^+ , X^0 , X^- AND X^{2-} QUANTUM DOT STATES

In the presence of a magnetic field, the emission lines from the X^+ to X^{2-} complexes split and shift. The QD emission energies E follow $E(B) = E(0) + \gamma_1 B + \gamma_2 B^2$.²⁸ In the case of X^0 , $\gamma_1 B$ describes the Zeeman effect and γ_2 is the diamagnetic coefficient. We first discuss in Section III.A the evolution of γ_2 with respect to θ and to the charge-state of the exciton. Then, we extract in Section III.B the electron and hole g -factors and the exchange energies for the different complexes.

A. Diamagnetic shift of the neutral and charged exciton complexes

We show in Figure 3 the angle dependence of γ_2 for X^0 , X^+ , X^- and X^{2-} . The diamagnetic shift of X^0 is given by $\gamma_2^{X^0} = e^2 \langle \rho^2 \rangle / 8\mu$,^{28,29} where μ and $\sqrt{\langle \rho^2 \rangle}$ are the exciton reduced mass and the exciton correlation length perpendicular to the axis of the applied magnetic field, respectively. As shown in Figure 3, $\gamma_2^{X^0}$ decreases from 8.5 to 4.0 $\mu\text{eV}/\text{T}^2$ when going from Faraday to Voigt geometry. Even if the hole mass anisotropy contributes slightly to the decrease of $\gamma_2^{X^0}$ when increasing θ , the θ -dependence of $\gamma_2^{X^0}$ arises mainly from the geometry of the investigated QD. The corresponding θ -dependence of $\sqrt{\langle \rho^2 \rangle}$ indicates that this QD exhibits a lens-shaped form. Conversely, as the shape of the exciton wave function is imposed by the QD geometry, this result confirms that the investigated excitons are strongly confined in the QD. For charged complexes, γ_2 is given by the diamagnetic shift of both the initial and the final states of the transition: it consequently provides some information on the relative spatial extent of these two states.^{14,15} First, X^+ and X^- exhibit a reduced γ_2 with increasing θ , as an indication that the symmetry of the wave functions of these complexes is imposed by the QD geometry. Second, X^+ , X^0 and X^- exhibit a similar γ_2 , indicating that the correlation length of a state involving an s -electron is insensitive to the presence of holes in the s -shell. In contrast to this insensitivity, for X^{2-} we observe a much smaller γ_2 . This shows that the p -electron wave function is sensitive to the presence of a hole in the QD: in the initial state of the transition, the hole binds the p -electron to the QD; after recombination the p -electron is more weakly confined and its wave function spreads more into the GaAs barriers. Finally, compared to X^0 and the trions, γ_2 for the X^{2-} shows a reduced anisotropy that arises from the delocalization of the p -electron inside the GaAs barriers.

B. Three-dimensional magneto-photoluminescence of neutral and singly charged excitons

We display in Figure 4 emission spectra from the neutral and negatively charged exciton complexes at zero magnetic field. The X^0 full width at half maximum (FWHM) is 71 μeV and no splitting is resolved. We therefore estimate that the anisotropic exchange splittings $|c_x + c_y|/2$ between the two bright states of X^0 is not larger than 30 μeV (c_x and c_y characterize the in-plane electron-hole spin-spin interaction),^{9,30} which indicates that the symmetry of the QD is nearly D_{2d} . We also neglect the anisotropic exchange splittings $|c_x - c_y|/2$ between the two dark X^0 states, as is usually done for InAs QDs.⁸ No fine structure is expected for the trion emission because of electron spin pairing, and as expected, for a given excitation density, the X^- emission is narrower

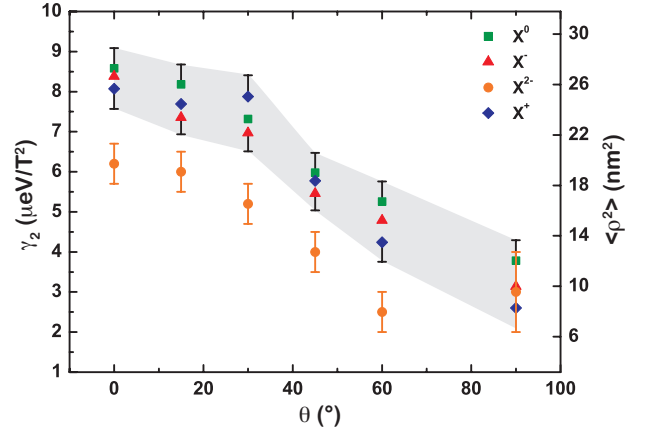


FIG. 3. (color online): Diamagnetic shift as a function of θ for an excitation density of $5 \times 10^9 \mu\text{W}/\text{cm}^2$ (for X^+ an excitation density of $60 \times 10^9 \mu\text{W}/\text{cm}^2$ was required). Experiments on X^+ , X^0 , X^- , X^{2-} have been taken with gate voltages of -0.78, -0.60, -0.30 and -0.04 V, respectively. On the right scale, the corresponding values for the square of the X^0 coherence length $\langle \rho^2 \rangle$ are shown.

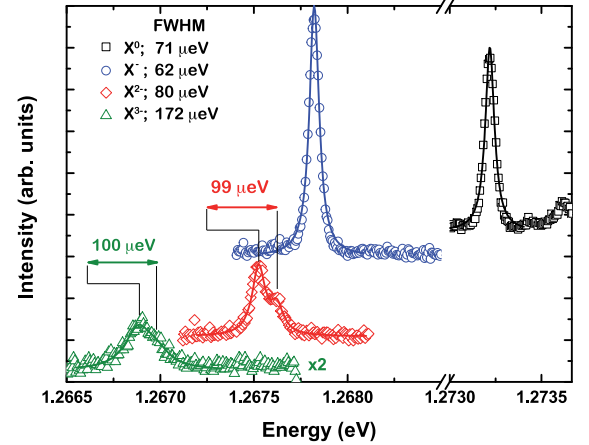


FIG. 4. (color online): PL spectra of the X^0 , X^- , X^{2-} and X^{3-} complexes (squares, circles, diamonds and triangles, respectively). Solid lines show the result of fitting with Lorentzian curves.

than the X^0 . Note that the 62 μeV linewidth measured for the X^- emission is likely to be given by spectral diffusion effects.³¹ The magnetic field-dependence of X^+ , X^0 and X^- emission energies for θ equal to 0, 45 and 90° are shown in Figure 5. In Faraday geometry, the emission from the X^0 bright states splits into two lines, whose energies $E_F^{X^0}$ follow:^{8,9}

$$E_F^{X^0}(B) = E_0 + \frac{c_z}{4} \pm \frac{1}{2} \mu_B B (g_e^{sz} + g_h^z) + \gamma_2^{X^0}(0^\circ) B^2. \quad (1)$$

g_e^{sz} and g_h^z are the s -electron and hole Landé factors along the dot axis, respectively, and $c_z/2$ is the isotropic exchange splitting.^{9,30} Away from Faraday geometry, the in-plane component of the magnetic field introduces some

mixing between the X^0 bright and dark states. Accordingly, two additional emission lines are observed for fields larger than about 2 T [Figure 5(b,c)]. In the specific case of Voigt geometry, the eigenenergies $E_{V,B}^{X^0}$ and $E_{V,D}^{X^0}$ of the primarily bright and dark states, respectively, are given by:^{8,32}

$$E_{V,B}^{X^0}(B) = E_0 + \frac{c_x}{4} \pm \frac{1}{2} \sqrt{\frac{[\mp(c_z - c_y)]^2}{4} + \mu_B^2 B^2 (g_h^x + g_e^{sx})^2} + \gamma_2^{X^0}(90^\circ) B^2, \quad (2)$$

and

$$E_{V,D}^{X^0}(B) = E_0 - \frac{c_x}{4} \pm \frac{1}{2} \sqrt{\frac{[\mp(c_z + c_y)]^2}{4} + \mu_B^2 B^2 (g_h^x - g_e^{sx})^2} + \gamma_2^{X^0}(90^\circ) B^2, \quad (3)$$

where g_e^{sx} and g_h^x are the s -electron and hole in-plane g -factors. While the data taken in Faraday and Voigt geometries were fitted using Equations (1-3), the data taken at intermediate θ were analyzed solving numerically the van Kesteren Hamiltonian.³³ Using the magnetic field dependence of X^0 emission energies for θ equal to 30, 45, 60 and 90°, we extract $c_z = 718 \pm 54 \mu\text{eV}$. This rather large c_z is in agreement with the fact that the investigated X^0 is strongly confined, c_z having been shown to scale like the inverse of the QD volume.⁸ Coming to the trions, their emission energies in Faraday geometry are given by:³⁴

$$E_F^{X^-,X^+}(B) = E_0 \pm \frac{\mu_B B}{2} |g_e^{sz} + g_h^z| + \gamma_2^{X^-,X^+}(0^\circ) B^2. \quad (4)$$

where $\gamma_2^{X^-}(\theta)$ and $\gamma_2^{X^+}(\theta)$ are the diamagnetic shifts of the negative and positive trions respectively. In Voigt geometry, the emission energies from the predominantly bright states are:³⁴

$$E_{V,B}^{X^-,X^+}(B) = E_0 \pm \frac{\mu_B B}{2} |g_e^{sx} + g_h^x| + \gamma_2^{X^-,X^+}(90^\circ) B^2, \quad (5)$$

and those from the predominantly dark states are:

$$E_{V,D}^{X^-,X^+}(B) = E_0 \pm \frac{\mu_B B}{2} |g_e^{sx} - g_h^x| + \gamma_2^{X^-,X^+}(90^\circ) B^2. \quad (6)$$

The magnetic field dependence of X^+ and X^- PL energies were fitted with the same approach than for X^0 . It is worth emphasizing that experiments performed in Voigt geometry do not allow for an accurate determination of g_e^x and g_h^x , the splittings between the different emission lines being too small. In view of this, experiments carried

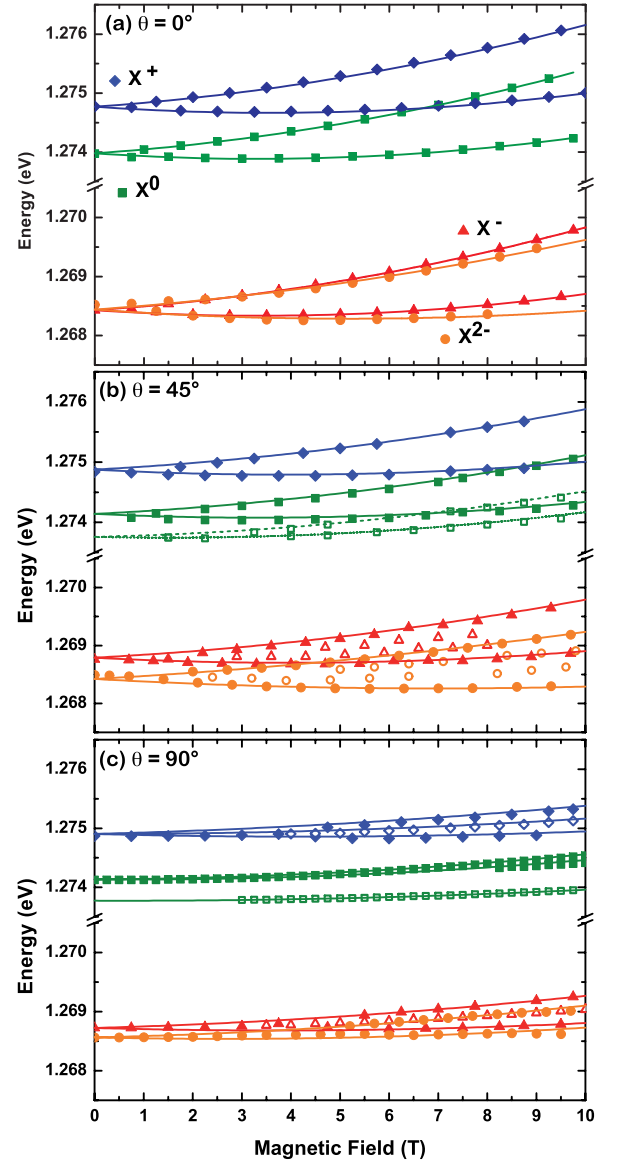


FIG. 5. (color online): Magnetic field-dependence of the PL energies of the X^+ , X^0 , X^- and X^{2-} complexes (diamonds, squares, triangles and circles, respectively) at 4.5 K for $\theta = 0^\circ, 45^\circ$ and 90° . Full and open symbols correspond to the emission from the primarily bright and dark states, respectively. In Faraday geometry, the X^+ , X^0 , X^- and X^{2-} magneto-PL spectra have been recorded at gate voltages of -0.78, -0.60, -0.30 and -0.04 V, respectively (comparable voltages were used for $\theta \neq 0$). Solid and dashed lines show the result of the fitting procedure of the emission energies of the predominantly bright and dark states, respectively.

out at $\theta = 45^\circ$ [Figure 5(b)] appear to yield the best balance between the emission intensity of the predominantly dark states and their energy splitting (splitting of about 200 μeV at 8 T). From the magnetic-field dependence of X^0 and the trions for $\theta = 0, 15, 30, 45, 60$ and 90° , we deduce $|g_e^{sx}| = 0.400 \pm 0.012$, $|g_e^{sz}| = 0.47 \pm 0.01$, $|g_h^x| = 0.020 \pm 0.001$ and $|g_h^z| = 1.50 \pm 0.05$. First, we manage

with this set of parameters to fit the X^0 , X^+ and X^- magneto-PL satisfactorily for all θ . The value deduced for $|g_e|$ is typical of InAs quantum dots^{16,32,35,36} and the slight anisotropy obtained for the g_e tensor confirms recent time-resolved pump-probe ellipticity experiments.³⁷ Concerning g_h , we attribute the small value of its in-plane component to the fact that the cubic terms in the spin Hamiltonian are negligible, as we previously showed in Ref.³². Regarding g_h^z , the values reported in the literature for InAs QDs are extremely scattered.^{32,35,36} This is usually assigned to the fact that g_h^z is a function of the heavy-hole light-hole mixing, the latter being strongly dependent on the shape, the composition and the strain state of the QD.^{38–41}

C. Three-dimensional magneto-photoluminescence of doubly negatively charged excitons

We present in this Section the behaviour of the PL from X^{2-} in the magnetic field for various θ . We only discuss here the magnetic-dependence of the recombination of X^{2-} into the triplet final state. The emission corresponding to the recombination into the singlet state is too weak for us to track its magnetic field-dependence. At zero magnetic field, the recombination into the triplet is composed of two lines (FWHM = 80 ± 2 μeV) split by 99 μeV (Figure 4). In contrast to the X^0 , both the $|\pm 1\rangle$ and the $|\pm 2\rangle$ states of the X^{2-} couple to the light at zero magnetic field (we still denote these states as bright and dark, respectively, in analogy with what done in Section III.B). The exchange interaction between the s -hole and the p -electron of the X^{2-} should in principle make it possible to resolve four distinct lines for the recombination into the triplet: (i) the isotropic exchange interaction splits energetically the bright and the dark states of X^{2-} by an amount $c_z^{sp}/2$ and (ii) the $|\pm 1\rangle$ states are further split by an amount that we take equal to $(c_x^{sp} + c_y^{sp})/2$. Following the approach taken in Refs.^{19,20}, we first neglect the exchange energy splitting between the $|\pm 2\rangle$ states. Then, and in contrast to the case of X^0 , $(c_x^{sp} + c_y^{sp})/2$ is typically 1.4 to 1.7 times larger than $c_z^{sp}/2$.^{19,20} We thus ascribe the lower energy line of the doublet to the recombination of the $|\pm 2\rangle$ and the $|-1\rangle$ states, while the higher energy one corresponds to the emission from the $|+1\rangle$ state.²⁰ We also deduce $(c_x^{sp} + c_y^{sp})/2 = 99$ μeV and $c_z^{sp}/2 = 65 \pm 6$ μeV , in agreement with previous reports.²⁰

The θ -dependent magneto-PL of the X^{2-} recombination is displayed in Figure 6. In Faraday geometry, the X^{2-} PL splits into two groups of two lines, each of them following a quadratic dependence on B . As in the case of the trion, a magnetic field splits both the initial and the final states involved in X^{2-} recombination. As a first approximation, Kazimierzuk *et al.* have taken similar g -factors for electrons in the s and the p shells, irrespective of the presence of a hole in the s -shell.¹⁹ As a result, in Faraday geometry, it follows straightforwardly

that the energy of the photons resulting from the recombination of the $|+2\rangle$ and the $|-1\rangle$ states should exhibit a Zeeman shift of $\mu_B|g_e^{sz} + g_h^z|B/2$. Similarly, we obtain that the linear shift of the emission from the $|-2\rangle$ and the $|+1\rangle$ X^{2-} would be $\mu_B|g_e^{sz} - g_h^z|B/2$. Now, the situation is made complicated by the fact that the p -electron envelope spreads into the GaAs barriers, this spreading depending on the presence of the hole in the s -shell (see Section III.A). Consequently, not only should the s - and the p -electron g -factors differ,^{42–44} but so will the p -electron g -factor for the initial and the final states of the X^{2-} recombination.⁴⁵ With $g_e^{pz,i}$ and $g_e^{pz,f}$ the p -electron g -factors of the initial and the final states of the X^{2-} recombination, the magnetic field dependence of the recombination energies of the X^{2-} dark states in Faraday geometry are given by:

$$E_{F,D}^{X^{2-}}(B) = E_0 - \frac{c_z^{sp}}{4} \pm \frac{\mu_B B}{2} (|g_e^{sz}| + |g_h^z| + |g_e^{pz,f} - g_e^{pz,i}|) + \gamma_2^{X^{2-}}(0^\circ)B^2 \quad (7)$$

where $g_e^{pz,i}$ and $g_e^{pz,f}$ are the p -electron g -factors for the initial and the final states of the X^{2-} recombination. In a similar manner, the emission energies for the recombination of the bright states into the triplet are:

$$E_{F,B}^{X^{2-}}(B) = E_0 + \frac{c_z^{sp}}{4} \mp \frac{1}{2}\mu_B B|g_e^{pz,f} - g_e^{sz}| + \gamma_2^{X^{2-}}(0^\circ)B^2 \pm \frac{1}{2}\sqrt{\frac{[\mp(c_x^{sp} + c_y^{sp})]^2}{4} + (\mu_B B|g_e^{pz,i} + g_h^z|)^2} \quad (8)$$

Using Equations (7) and (8) to fit the data in Figure 6(a) (we take g_e^{sz} , g_h^z , c_z^{sp} , $(c_x^{sp} + c_y^{sp})/2$ and $\gamma_2^{X^{2-}}(\theta)$ as determined above), we get $|g_e^{pz,f} - g_e^{pz,i}| = 0.12$ [the result of the fitting is shown in Figure 5(a)]. We tentatively attribute the increase in the absolute value of g_e^{pz} to the spreading of the p -electron wave function into the GaAs barriers after the X^{2-} recombination. Now, following this latter assumption we can consider $g_e^{pz,i} = g_e^{sz}$ and given that g_e^{sz} is likely to be negative,⁴⁶ it comes that $g_e^{pz,f} = -0.59$. Since the electron g -factor in unstrained bulk GaAs is -0.44,⁴⁷ the value found for $g_e^{pz,f}$ might at first appear surprising. However, the potential barrier between the QD and the barriers is not sharp since there is some alloy intermixing between the InAs QD and the GaAs barriers.⁴⁸ As a consequence, the p -electron wave function probes a low In-content (In,Ga)As alloy rather than pure GaAs, implying a deviation of the g -factor value.

When a magnetic field with an in-plane component is applied, the initial and the final states of the X^{2-} recombination get mixed. Accounting for the different channels available for the recombination of each of the four X^{2-} states, we now expect to detect twelve distinct emission lines. Nevertheless, as shown in Figure 6(b,c) for $\theta = 45^\circ$

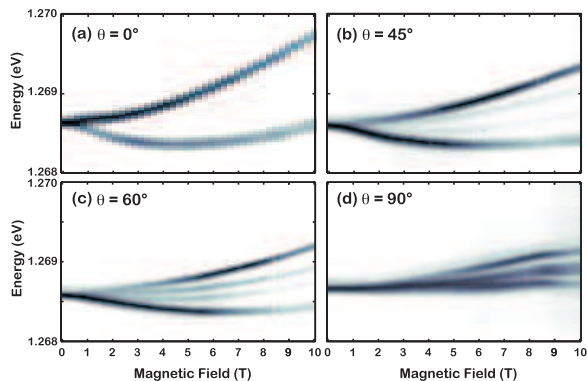


FIG. 6. (color online): Magneto-PL of the doubly negatively charged exciton for $\theta = 0$ (a), 30 (b), 45 (c) and 90° (d). (a) In Faraday geometry, two emission lines are resolved. (b)-(d) For non-zero θ , the mixing between bright and dark states makes it possible to observe four distinct emission lines. In this tilted state, for fields larger than about 8 T the asymmetry of diamagnetic forces in the apparatus is sufficient to alter slightly the optical alignment of the system, resulting in a decrease in emission intensity for all emission lines.

and 60° , only four groups of two lines are resolved, the four remaining transitions carrying a too weak oscillator strength to be detected. Similarly to what seen for X^0 and the trions and in agreement with magneto-PL experiments on X^{2-} in CdTe/ZnTe QDs,¹⁹ the Zeeman splittings reduce with increasing θ and it gets almost impossible to resolve the multiple splittings of the emission lines in Voigt geometry [Figure 6(d)]. In addition, any quantitative discussion of the Zeeman splittings at intermediate θ is hindered by the fact that (i) g_e^{pz} and g_e^{px} depends on the spreading of the p -electron wave function in the barriers and (ii) the shape of the p -electron wave function strongly depends on the field orientation.⁴³

V. ANGLE-DEPENDENT HYBRIDIZATION OF ELECTRONIC QUANTUM DOT STATES WITH THE WETTING LAYER

We now turn our attention to the magneto-PL from the triply negatively charged exciton X^{3-} . The two p -electrons of this complex may occupy either a different or the same sub-shell. In the case of QDs with in-plane isotropy, the p_x and p_y states are degenerate and the X^{3-} exhibits an open-shell configuration: both the p_x and the p_y states are occupied and the two p -electrons have parallel spins. The open-shell X^{3-} may recombine into a triplet or a singlet state, giving rise to two emission bands split by electron-electron exchange interaction.²³ As was the case for the X^{2-} , we will not comment further on the recombination of the X^{3-} into the singlet because of the relatively low intensity of this emission.²³ In presence of in-plane anisotropy, the degeneracy between the p_x and the p_y states is lifted. When the in-plane anisotropy is

such that the energy separation between the p_x and the p_y states is larger than the exchange energy between the p_x and p_y electrons, both p -electrons occupy the lower-energy subshell.⁴⁹ the X^{3-} is said to adopt a closed-shell configuration. Note that the observation at zero magnetic-field of the closed-shell X^{3-} does not necessarily imply that the QD exhibits an in-plane anisotropy. For instance, the presence of electrons in the wetting layer is sufficient to break the potential symmetry in the QD and to favour the closed-shell configuration.^{50,51}

The emission spectra from the X^{3-} at zero-magnetic field is shown in Figure 7. It is dominated by an emission band centered at 1267.9 meV that we attribute to the recombination of the open-shell X^{3-} into the triplet. The open-shell X^{3-} emission shows a fine structure (Figure 4), as a result of exchange interaction between the s -hole and the p -electrons.^{49,51} While the 100 μ eV exchange splitting observed here between the open-shell X^{3-} states is similar to what reported in Refs.^{49,51} (Figure 4), the emission lines appeared to be much broader (FWHM = 170 μ eV against ca 70 μ eV in Refs.^{49,51}). We observe a much weaker and broader (FWHM = 790 μ eV) emission band centered at 1266.5 meV [Figure 7(e)], that we ascribe to the recombination of the closed-shell X^{3-} .⁵² As shown in Figure 8, after recombination of the closed-shell X^{3-} , the QD is in an excited state. Fast reconfiguration of the final state occurs by Auger process and results in the large emission broadening observed in Figure 7. We emphasise that the electron promoted to the d -shell couples to the wetting layer.^{52,53} The three-dimensional behaviour of the magneto-PL of the closed-shell X^{3-} , the so-called Kondo-Anderson excitons,^{53,54} will be discussed in the remainder of this paper.

The evolution of the X^{3-} emission energies in a magnetic field at $\theta = 0$ is quite different from what observed so far for less-charged complexes [Figure 7(a)]. First, when increasing the magnetic field, the emission from the open-shell X^{3-} quenches in favour of the closed-shell one. Applying a magnetic field splits the p_x and p_y subshells, making the closed-shell configuration energetically more favourable.⁵⁰ With I_{cs} and I_{tot} the emission intensity from the closed-shell X^{3-} and the total X^{3-} emission intensity, respectively, we define the spin-flip magnetic field B_{sf} as the field at which $\frac{I_{cs}}{I_{tot}} = 1 - \frac{1}{e} [1 - \frac{I_{cs}(0)}{I_{tot}(0)}]$. We measure $B_{sf} = 2.44 \pm 0.1$ T [Figure 7(g)]. Second, the emission from the closed-shell X^{3-} does not follow a parabolic dependence with increasing magnetic field [Figure 7(a,e)]. In agreement with earlier works,^{6,50,51} the closed-shell X^{3-} emission shows several anticrossings for intermediate values of the magnetic field ranging between 2 and 8 T. This is the signature of the hybridization between localized (QD with full p -shell and one electron in the s -shell) and extended states (QD with full s -shell and one electron delocalized in the wetting layer).⁶ We underline that the asymptotes of the closed-shell X^{3-} emission energies are linear with the magnetic field, as a result of the development of the wetting layer continuum of states into Landau levels. At resonance be-

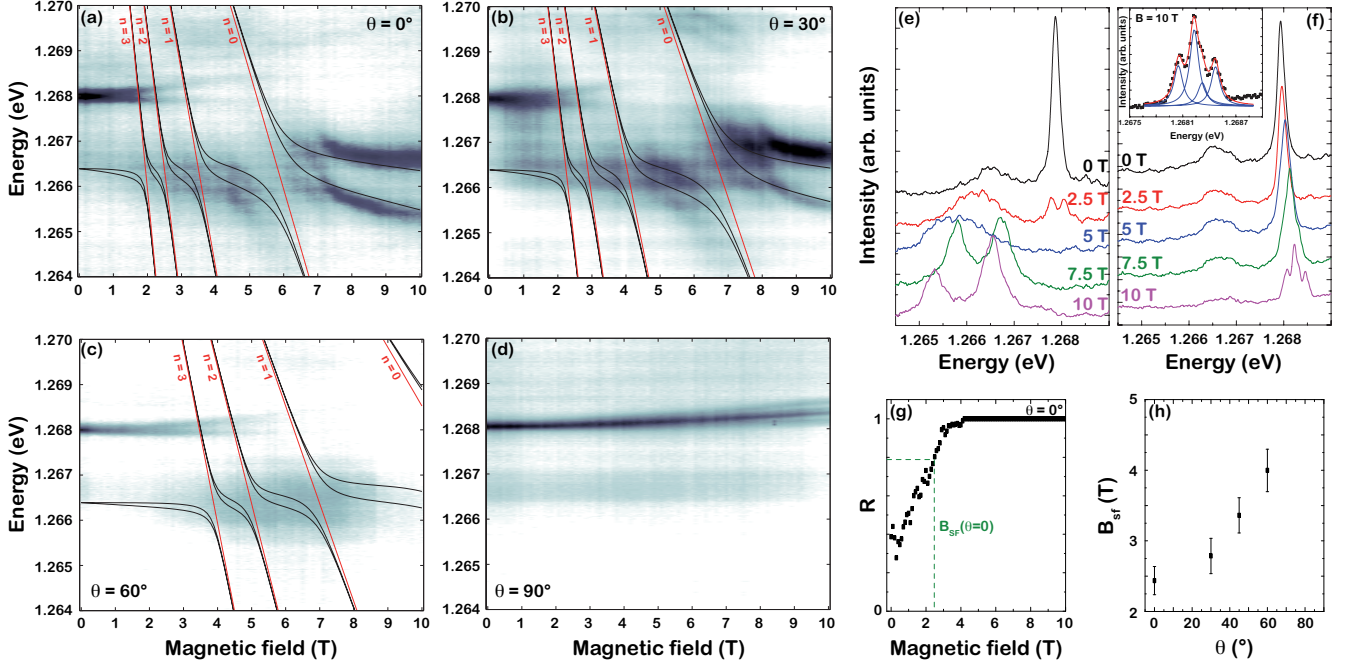


FIG. 7. (color online): (a)-(d) Magneto-photoluminescence intensity maps versus photon energy and magnetic field of the X^{3-} taken at $\theta = 0$ (a), 30° (b), 60° (c) and 90° (d). Solid lines in (a-c) show the result of the fitting accounting for the coupling between the final state of the X^{3-} recombination and the electron Landau levels of the wetting layer. (e,f) PL spectra of the X^{3-} taken at 0, 2.5, 5, 7.5 and 10 T in Faraday (e) and Voigt (f) geometries. The inset in (f) shows that the emission of the X^{3-} in Voigt geometry splits into four components. The red line shows the result of a deconvolution of the spectrum using four Lorentzian curves with a FWHM of $120 \mu\text{eV}$ (blue lines). (g) Ratio R between the emission intensity from the closed-shell X^{3-} and the total X^{3-} emission intensity with respect to the magnetic field. We define as B_{sf} the magnetic field at which $R = 1 - [1 - R(0)]/\exp(1)$ (green dashed line). (h) Evolution of B_{sf} with respect to θ .

tween the localized and the delocalized electronic states, $\Delta = (n + 3/2)e\hbar B/m_e$, where m_e is the electron effective mass in the wetting layer, n the index for the n^{th} Landau level and Δ the kinetic energy at zero field of the electron in the wetting layer.⁵⁰ Using $m_e = 0.067m_0$, we obtain $\Delta = 15 \pm 1 \mu\text{eV}$. Concerning the asymptotes themselves, their magnetic field dependences are given by:⁶

$$E_0 + \Delta - (n + \frac{3}{2})e\hbar B/m, \quad (9)$$

where E_0 is the emission energy from the closed-shell X^{3-} at zero field. For magnetic fields larger than 8 T, the final state of the X^{3-} recombination is fully localized into the QD. As the initial and the final states of the recombination are influenced by the magnetic field only through coupling to the spins of the s -hole and the s -electron, respectively, the closed-shell emission is split into two components whose energy separation is proportional to $|g_e^{sz} - g_h^z|B$. In addition, we deduce from Figure 7(e) a paramagnetic behaviour (i.e. $\gamma_2 < 0$) for the closed-shell X^{3-} . According to our previous discussions in Sections IV.A and IV.C, this observation confirms that the extent into the GaAs barriers of the p -electron envelope is larger for the final state than for the initial state of the recombination.

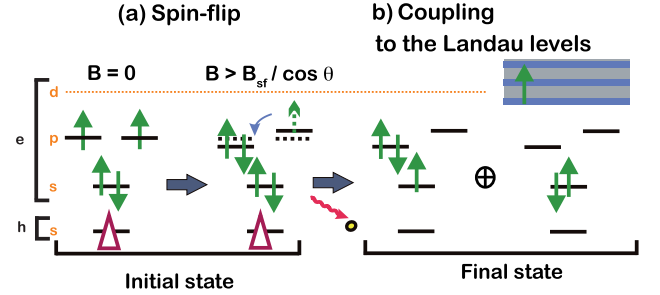


FIG. 8. (color online) (a) Applying a magnetic field parallel to the quantum dot high symmetry axis splits the p_x and p_y subshells, favouring the closed-shell X^{3-} against the open-shell one. (b) After recombination of the closed-shell X^{3-} , the QD is in an excited state. Auger interaction promotes an electron into the d -shell, which couples with wetting layer states. In presence of magnetic field, the wetting layer continuum of states develops into Landau levels, giving rise to the anticrossings seen in Figure 7(a-c). This figure follows the scheme outlined by Karrai *et al.*⁶

Some remarkable changes occur when the magnetic field is tilted with respect to the growth axis. First, as displayed in Figure 7(a-d,h), B_{sf} increases with θ . We emphasize that in Voigt geometry, the emission from the

open-shell X^{3-} dominates the spectrum over the whole range of investigated magnetic fields. To explain this observation, we consider the evolution of the energy spectrum of a QD in a tilted magnetic field. This generalised version of the Fock-Darwin problem has been solved analytically in Ref.⁵⁵. In this work, Henriques and Efros predict for a given value of the magnetic field a reduced splitting between the p_x and p_y states as θ is increased. It follows that B_{sf} increases with θ , in agreement with the data in Figure 7(h). Second, the slope of the asymptotes of the closed-shell X^{3-} emission energies decrease with θ [Figure 7(a-c)]. In particular, when $\theta = 90^\circ$, the magnetic field-dependence of the closed-shell X^{3-} emission energies exhibit no anticrossing [Figure 7(d,f)]. We attribute such a decrease in the slopes of the asymptotes to the fact that the eigenenergies for an electron in a quantum well in presence of a tilted magnetic field are proportional to the component of the magnetic field parallel to the confinement axis.⁵⁶ In agreement, the asymptotes in Figure 7(b,c) are fitted fairly well using Equation (9) with B the on-axis component of the applied magnetic field. We underline that tuning θ and the amplitude of the magnetic field modifies the shape of the wave function of electrons confined in the QD,⁴³ which opens the possibility of studying different configurations of Kondo-Anderson states. When $\theta = 90^\circ$, both the open-shell and the closed-shell X^{3-} emission energies exhibit a quadratic behaviour with magnetic field, as an indication that the X^{3-} can now be treated in the artificial atom model. For instance, at 10 T, the open-shell X^{3-} emission splits into four lines, as a result of the Zeeman effect on both the initial and the final state of the recombination. Concerning, the X^{3-} in the closed-shell configuration, its emission energy in Voigt geometry shows almost no dependence on the magnetic field: no

splitting is resolved and $\gamma_2 = 0.5 \mu\text{eV}/T^2$.

VI. CONCLUSIONS

In conclusion, we have carried out three-dimensional magneto-photoluminescence experiments on neutral and charged excitons in InAs/GaAs quantum dots. Performing magneto-photoluminescence with different field orientation not only allows estimating the shape of the exciton wave function, but also makes it possible to determine accurately the Landé g -tensors for electrons and holes in the s -shell. Experiments on doubly and triply negatively charged excitons provide information on carriers in high-energy shells. In particular, we have demonstrated that the g -factor of the p -electron depends strongly on the spreading of its wave function inside the dot barriers and on the presence of the hole in the s -shell. Finally, we have observed coherent coupling between the quantum dot electronic states and the wetting layer Landau levels. We have investigated the magnetic field-dependence of this coupling for various orientations of the magnetic field. Then, based on the energy spectrum of electrons in quantum dot in tilted magnetic fields, we have shown that when increasing the angle between the magnetic field and the dot high symmetry axis, the system evolves from a Kondo-Anderson exciton description to the artificial atom model.

ACKNOWLEDGMENTS

We acknowledge funding from the EPSRC. B.V.H also thanks the Hitachi Cambridge Laboratory for additional funding. P.C. acknowledges financial support from the European Union Seventh Framework Programme under Grant Agreement No. 265073.

* bv252@cam.ac.uk

† Present address: Navy Research Laboratory, Electronic Materials Branch, Code 6877 4555 Overlook Ave. SW, Washington, DC 20375

‡ Present address: Centre de Recherche sur l'Hétéro-Epitaxie et ses Applications, Centre National de la Recherche Scientifique (CRHEA-CNRS), Parc Sophia Antipolis, Rue Bernard Grégory, 06560 Valbonne, France

¹ P. Michler, A. Kiraz, C. Becher, W. V. Schoenfeld, P. M. Petroff, L. Zhang, E. Hu, and A. Imamoglu, *Science* **290**, 2282 (2000).

² N. Akopian, N. H. Lindner, E. Poem, Y. Berlatzky, J. Avron, D. Gershoni, B. D. Gerardot, and P. M. Petroff, *Phys. Rev. Lett.* **96**, 130501 (2006).

³ R. M. Stevenson, R. J. Young, P. Atkinson, K. Cooper, D. A. Ritchie, and A. J. Shields, *Nature* **439**, 179 (2006).

⁴ X. Li, Y. Wu, D. Steel, D. Gammon, T. H. Stievater, D. S. Katzer, D. Park, C. Piermarocchi, and L. J. Sham, *Science* **301**, 809 (2003).

⁵ S. Sasaki, S. De Franceschi, J. M. Elzerman, W. G. van der Wiel, M. Eto, S. Tarucha, and L. P. Kouwenhoven, *Nature* **405**, 764 (2000).

⁶ K. Karrai, R. J. Warburton, C. Schulhauser, A. Högele, B. Urbaszek, E. J. McGhee, A. O. Govorov, J. M. Garcia, B. D. Gerardot, and P. M. Petroff, *Nature* **427**, 135 (2004).

⁷ P. A. Dalgarno, M. Ediger, B. D. Gerardot, J. M. Smith, S. Seidl, M. Kroner, K. Karrai, P. M. Petroff, A. O. Govorov, and R. J. Warburton, *Phys. Rev. Lett.* **100**, 176801 (2008).

⁸ M. Bayer, G. Ortner, O. Stern, A. Kuther, A. A. Gorbunov, A. Forchel, P. Hawrylak, S. Fafard, K. Hinzer, T. L. Reinecke, S. N. Walck, J. P. Reithmaier, F. Kloppe, and F. Schäfer, *Phys. Rev. B* **65**, 195315 (2002).

⁹ A. G. Steffan and R. T. Phillips, *Phys. Stat. Sol. (a)* **190**, 541 (2002).

¹⁰ N. I. Cade, H. Gotoh, H. Kamada, H. Nakano, and H. Okamoto, *Phys. Rev. B* **73**, 115322 (2006).

- ¹¹ H. Sanada, T. Sogawa, H. Gotoh, Y. Tokura, H. Yamaguchi, H. Nakano, and H. Kamada, Phys. Rev. B **79**, 121303 (2009).
- ¹² M. Abbarchi, T. Kuroda, T. Mano, K. Sakoda, and M. Gurioli, Phys. Rev. B **81**, 035334 (2010).
- ¹³ B. J. Witek, R. W. Heeres, U. Perinetti, E. P. A. M. Bakkers, L. P. Kouwenhoven, and V. Zwiller, Phys. Rev. B **84**, 195305 (2011).
- ¹⁴ C. Schulhauser, D. Haft, R. J. Warburton, K. Karrai, A. O. Govorov, A. V. Kalameitsev, A. Chaplik, W. Schoenfeld, J. M. Garcia, and P. M. Petroff, Phys. Rev. B **66**, 193303 (2002).
- ¹⁵ Y. J. Fu, S. D. Lin, M. F. Tsai, H. Lin, C. H. Lin, H. Y. Chou, S. J. Cheng, and W. H. Chang, Phys. Rev. B **81**, 113307 (2010).
- ¹⁶ W. Sheng, S. J. Xu, and P. Hawrylak, Phys. Rev. B **77**, 241307 (2008).
- ¹⁷ G. Sallen, B. Urbaszek, M. M. Glazov, E. L. Ivchenko, T. Kuroda, T. Mano, S. Kunz, M. Abbarchi, K. Sakoda, D. Lagarde, A. Balocchi, X. Marie, and T. Amand, Phys. Rev. Lett. **107**, 166604 (2011).
- ¹⁸ D. Y. Oberli, Phys. Rev. B **85**, 155305 (2012).
- ¹⁹ T. Kazimierzczuk, T. Smoleński, M. Goryca, L. Kłopotowski, P. Wojnar, K. Fronc, A. Golnik, M. Nawrocki, J. A. Gaj, and P. Kossacki, Phys. Rev. B **84**, 165319 (2011).
- ²⁰ M. Ediger, G. Bester, B. D. Gerardot, A. Badolato, P. M. Petroff, K. Karrai, A. Zunger, and R. J. Warburton, Phys. Rev. Lett. **98**, 036808 (2007).
- ²¹ M. Ediger, G. Bester, A. Badolato, P. Petroff, K. Karrai, A. Zunger, and R. Warburton, Nature Physics **3**, 774 (2007).
- ²² T. Kehoe, M. Ediger, R. T. Phillips, and M. Hopkinson, Rev. Sci. Instrum. **81**, 013906 (2010).
- ²³ R. J. Warburton, C. Schäflein, D. J. Haft, F. Bickel, A. Lorke, K. Karrai, J. M. Garcia, W. Schoenfeld, and P. M. Petroff, Nature **405**, 926 (2000).
- ²⁴ F. Findeis, M. Baier, A. Zrenner, M. Bichler, G. Abstreiter, U. Hohenester, and E. Molinari, Phys. Rev. B **63**, 121309 (2001).
- ²⁵ J. J. Finley, P. W. Fry, A. D. Ashmore, A. Lemaître, A. I. Tartakovskii, R. Oulton, D. J. Mowbray, M. S. Skolnick, M. Hopkinson, P. D. Buckle, and P. A. Maksym, Phys. Rev. B **63**, 161305 (2001).
- ²⁶ E. Poem, J. Shemesh, I. Marderfeld, D. Galushko, N. Akopian, D. Gershoni, B. D. Gerardot, A. Badolato, and P. M. Petroff, Phys. Rev. B **76**, 235304 (2007).
- ²⁷ M. Ediger, P. A. Dalgarno, J. M. Smith, B. D. Gerardot, R. J. Warburton, K. Karrai, and P. M. Petroff, Appl. Phys. Lett. **86**, 211909 (2005).
- ²⁸ S. N. Walck and T. L. Reinecke, Phys. Rev. B **57**, 9088 (1998).
- ²⁹ K. J. Nash, M. S. Skolnick, P. A. Claxton, and J. S. Roberts, Phys. Rev. B **39**, 10943 (1989).
- ³⁰ R. T. Phillips, A. G. Steffan, S. R. Newton, T. L. Reinecke, and R. Kotlyar, Phys. Stat. Sol. (b) **238**, 601 (2003).
- ³¹ I. Favero, A. Berthelot, G. Cassabois, C. Voisin, C. Delalande, P. Roussignol, R. Ferreira, and J. M. Gérard, Phys. Rev. B **75**, 073308 (2007).
- ³² I. Toft and R. T. Phillips, Phys. Rev. B **76**, 033301 (2007).
- ³³ H. W. van Kesteren, E. C. Cosman, W. A. J. A. van der Poel, and C. T. Foxon, Phys. Rev. B **41**, 5283 (1990).
- ³⁴ J. G. Tischler, A. S. Bracker, D. Gammon, and D. Park, Phys. Rev. B **66**, 081310 (2002).
- ³⁵ D. N. Krizhanovskii, A. Ebbens, A. I. Tartakovskii, F. Pulizzi, T. Wright, M. S. Skolnick, and M. Hopkinson, Phys. Rev. B **72**, 161312 (2005).
- ³⁶ D. Y. Oberli, M. Byszewski, B. Chalupar, E. Pelucchi, A. Rudra, and E. Kapon, Phys. Rev. B **80**, 165312 (2009).
- ³⁷ G. Sallen, B.-M. Meiners, A. Greilich, D. R. Yakovlev, M. Bayer, A. D. B. Maia, A. A. Quivy, and A. B. Henriques, Appl. Phys. Lett. **99**, 221914 (2011).
- ³⁸ T. Nakaoka, T. Saito, J. Tatebayashi, S. Hirose, T. Usuki, N. Yokoyama, and Y. Arakawa, Phys. Rev. B **71**, 205301 (2005).
- ³⁹ A. Babinski, G. Ortner, S. Raymond, M. Potemski, M. Bayer, W. Sheng, P. Hawrylak, Z. Wasilewski, S. Fafard, and A. Forchel, Phys. Rev. B **74**, 075310 (2006).
- ⁴⁰ W. Sheng and A. Babinski, Phys. Rev. B **75**, 033316 (2007).
- ⁴¹ W. Sheng, Physica E: Low-dimensional Systems and Nanostructures **41**, 1 (2007).
- ⁴² I. A. Akimov, K. V. Kavokin, A. Hundt, and F. Henneberger, Phys. Rev. B **71**, 075326 (2005).
- ⁴³ T. P. M. Alegre, F. G. G. Hernández, A. L. C. Pereira, and G. Medeiros-Ribeiro, Phys. Rev. Lett. **97**, 236402 (2006).
- ⁴⁴ T. Kazimierzczuk, M. Goryca, P. Wojnar, A. Golnik, M. Nawrocki, and P. Kossacki, Acta Physica Polonica A **120**, 874 (2011).
- ⁴⁵ A. A. Kiselev, E. L. Ivchenko, and U. Rössler, Phys. Rev. B **58**, 16353 (1998).
- ⁴⁶ C. E. Pryor and M. E. Flatté, Phys. Rev. Lett. **96**, 026804 (2006).
- ⁴⁷ M. Oestreich and W. W. Rühle, Phys. Rev. Lett. **74**, 2315 (1995).
- ⁴⁸ G. Vastola, Y.-W. Zhang, and V. B. Shenoy, Current Opinion in Solid State and Materials Science **16**, 64 (2012).
- ⁴⁹ B. Urbaszek, R. J. Warburton, K. Karrai, B. D. Gerardot, P. M. Petroff, and J. M. Garcia, Phys. Rev. Lett. **90**, 247403 (2003).
- ⁵⁰ R. J. Warburton, B. Urbaszek, E. J. McGhee, C. Schulhauser, A. Högele, K. Karrai, A. O. Govorov, J. M. Garcia, B. D. Gerardot, and P. M. Petroff, MRS Proceedings **737**, E12.1 (2003).
- ⁵¹ R. Warburton, B. Urbaszek, E. McGhee, C. Schulhauser, A. Högele, K. Karrai, B. Gerardot, and P. Petroff, Physica E: Low-dimensional Systems and Nanostructures **26**, 45 (2005).
- ⁵² A. Govorov, K. Karrai, R. Warburton, and A. Kalameitsev, Physica E: Low-dimensional Systems and Nanostructures **20**, 295 (2003).
- ⁵³ A. O. Govorov, K. Karrai, R. J. Warburton, and A. V. Kalameitsev, MRS Proceedings **737**, E12.5 (2003).
- ⁵⁴ A. O. Govorov, K. Karrai, and R. J. Warburton, Phys. Rev. B **67**, 241307 (2003).
- ⁵⁵ A. B. Henriques and A. L. Efros, Phys. Rev. B **80**, 153302 (2009).
- ⁵⁶ G. Bastard, *Wave mechanics applied to semiconductor heterostructures*, Monographies de physique (Les Editions de Physique, 1988).